

## Wettability of graphene-laminated micropillar structures

Jihye Bong, Keumyoung Seo, Ji-Hoon Park, Joung Real Ahn, and Sanghyun Ju

Citation: *Journal of Applied Physics* **116**, 234303 (2014); doi: 10.1063/1.4904353

View online: <http://dx.doi.org/10.1063/1.4904353>

View Table of Contents: <http://scitation.aip.org/content/aip/journal/jap/116/23?ver=pdfcov>

Published by the [AIP Publishing](#)

---

### Articles you may be interested in

[The tunable wettability in multistimuli-responsive smart graphene surfaces](#)

*Appl. Phys. Lett.* **102**, 011603 (2013); 10.1063/1.4775360

[Wettability of pristine and alkyl-functionalized graphane](#)

*J. Chem. Phys.* **137**, 034707 (2012); 10.1063/1.4732520

[Retraction: "Influence of surface topography and chemical structure on wettability of electrodeposited ZnO thin films" \[\*J. Appl. Phys.\* 108, 083507 \(2010\)\]](#)

*J. Appl. Phys.* **110**, 039901 (2011); 10.1063/1.3615932

[Influence of surface topography and chemical structure on wettability of electrodeposited ZnO thin films](#)

*J. Appl. Phys.* **108**, 083507 (2010); 10.1063/1.3493735

[Intrinsic slip on hydrophobic self-assembled monolayer coatings](#)

*Phys. Fluids* **22**, 042003 (2010); 10.1063/1.3394120

---



## Wettability of graphene-laminated micropillar structures

Jihye Bong,<sup>1</sup> Keumyoung Seo,<sup>1</sup> Ji-Hoon Park,<sup>2</sup> Joung Real Ahn,<sup>2,a)</sup> and Sanghyun Ju<sup>1,a)</sup>

<sup>1</sup>Department of Physics, Kyonggi University, Suwon, Gyeonggi-Do 443-760, South Korea

<sup>2</sup>Department of Physics, Sungkyunkwan University, Suwon, Gyeonggi-Do 440-746, South Korea

(Received 18 September 2014; accepted 4 December 2014; published online 18 December 2014)

The wetting control of graphene is of great interest for electronic, mechanical, architectural, and bionic applications. In this study, the wettability of graphene-laminated micropillar structures was manipulated by changing the height of graphene-laminated structures and employing the trichlorosilane (HDF-S)-based self-assembly monolayer. Graphene-laminated micropillar structures with HDF-S exhibited higher hydrophobicity (contact angle of 129.5°) than pristine graphene thin film (78.8°), pristine graphene-laminated micropillar structures (97.5°), and HDF-S self-assembled graphene thin film (98.5°). Wetting states of the graphene-laminated micropillar structure with HDF-S was also examined by using a urea solution, which flowed across the surface without leaving any residues.

© 2014 AIP Publishing LLC. [<http://dx.doi.org/10.1063/1.4904353>]

### INTRODUCTION

Graphene, with its two-dimensional honeycomb crystal structure consisting of sp<sup>2</sup>-hybridized carbon, is a promising material for electrical, energy, and environmental applications because of its high mobility and conductivity as well as its mechanical flexibility and optical transparency. In this regard, there have been attempts to develop high-performance field-effect transistors, photo-detectors, photo-transistors, and hot-electron bolometers by modifying the electrical, optical, and thermal characteristics of graphene.<sup>1–5</sup> There have also been attempts to apply graphene to control the wettability of a surface, since graphene has a relatively high hydrophobicity, in addition to studies on the antibacterial effect of graphene, in which the survival of bacteria on graphene was analyzed as a function of time.<sup>6,7</sup>

In order to control wettability for industrial and scientific applications, many studies have been conducted on tuning the surface energy, one way of doing which is modifying surface roughness or incorporation of a self-assembly monolayer on a surface.<sup>8–12</sup> It is well known that an increase in surface roughness and an application of a self-assembly monolayer on a surface drive a decrease in the surface energy and consequently lead to enhanced hydrophobicity.<sup>13–15</sup> In this context, some studies on the control of hydrophobic and omniphobic properties have been conducted using hydrophilic polymer materials, porous Teflon membranes, epoxy-based nanostructured surfaces, and nanowires with lubricants.<sup>16,17</sup> Recently, the control of wettability in graphene thin films by modifying the graphene surface and the number of graphene layers was reported.<sup>18–21</sup> However, the control of wettability by adjusting three-dimensional structures of graphene laminates has not yet been reported.

In this study, we demonstrated the wettability control of graphene-laminated micropillar structures with changing the heights of micropillar structures and employing

(heptadecafluoro-1,1,2,2-tetrahydrodecyl)trichlorosilane (HDF-S)-based self-assembled monolayers. The contact angle characteristics of the following four different surfaces were compared: the pristine graphene thin film, the HDF-S self-assembled graphene thin film, the pristine graphene on the micropillar structure, and the HDF-S self-assembled graphene on the micropillar structure. A change of wetting properties upon increasing the height of graphene micropillar structures was observed by contact angle measurements. The flow of urea solution on the graphene-laminated micropillar structure with HDF-S was also examined.

### EXPERIMENTAL

Figure 1 shows the schematic of the transfer process for forming graphene-laminated micropillar structures. Microscale pillar structures were fabricated by using a conventional photolithography process. Dry etching was performed for patterning micropillar structures under a RF power of 100 W and a CF<sub>4</sub> gas of 10 sccm. In order to improve the adhesion of graphene on the micropillar structures, indium tin oxide (ITO, t ~ 100 nm) was deposited on the silicon-based micropillar structures. Graphene, grown on a Cu foil through the chemical vapor deposition (CVD) method, was transferred by using poly(methyl methacrylate) (PMMA). After coating the PMMA on a top surface of graphene, Cu was removed using a Cu etchant (CE-100 from Transene Company) and rinsed off with deionized (DI) water three times. In order to remove the residue of Cu completely, the PMMA/graphene substrate was immersed in nitric acid for 10 min, and rinsed off with DI water. The prepared PMMA/graphene was transferred to a micropillar-patterned substrate and then dried in an oven at 80 °C. To increase the adsorption capacity of the graphene on the substrate, another PMMA coating was applied on the PMMA/graphene/micropillar-patterned substrate, which was then dried on a hot plate at 130 °C, approximately the melting point of PMMA. The PMMA melted during the process and consequently applied downward pressure on the graphene, enabling the adsorption of the graphene along the shape of substrate.<sup>22,23</sup> A thermal annealing method was employed to

<sup>a)</sup>Authors to whom correspondence should be addressed. Electronic addresses: jrahn@skku.edu and shju@kgu.ac.kr

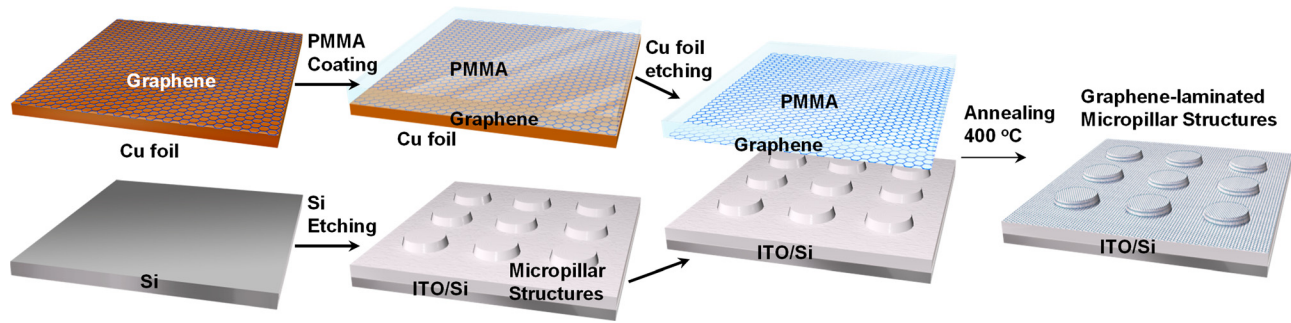


FIG. 1. Process for transfer of graphene onto a micro-pillar patterned substrate.

remove the PMMA,<sup>24</sup> since the previous removal method with acetone might have promoted weak adhesion, cracks, or wrinkles in graphene.<sup>22</sup> The PMMA removal process was carried out at  $3 \times 10^{-3}$  Torr at 400 °C for 20 min.

For the self-assembly of trichlorosilane-based self-assembly monolayer (SAM), graphene-laminated micropillar substrates were cleaned with isopropyl alcohol through agitation to remove organic contaminants and improve self-assembly. They were then immersed in a 3.0 mM of HDF-S in anhydrous toluene in an atmosphere of nitrogen for 1 h. After completing the reaction for 1 h, the substrates were rinsed with fresh solution of toluene and isopropyl alcohol, and subsequently dried under nitrogen gas. The method specified above was applied three times to form tri-layered graphene. Tri-layered graphene was laminated on three-dimensional micropillar structures in order to avoid the defects generated during first or second graphene lamination. Thus, the reliable contact angles values could be uniformly obtained. The surface topology of the graphene-laminated micropillar structure with HDF-S was observed using a field emission scanning electron microscope (FE-SEM). The self-assembly of HDF-S on graphenes was analyzed by an attenuated total reflectance Fourier transform infrared spectroscopy (ATR-FTIR). To verify the contact angles of the fabricated substrates, water droplets ( $5 \mu\text{l}$ ) were dropped onto the surface of the fabricated substrates (room temperature, ambient air, and Phoenix 300).

## RESULTS AND DISCUSSION

Figure 2(a) shows the representative FE-SEM image of the graphene-laminated micropillar array, with each micropillar having a diameter of  $\sim 7 \mu\text{m}$ , a pitch of  $\sim 33 \mu\text{m}$ , and a height of  $\sim 5.1 \mu\text{m}$ . Micropillar structures with a truncated cone shape were produced by photolithography and dry-etching processes. Single-layer graphene grown on a Cu foil by a CVD was transferred onto the micropillar-patterned substrate three times. The inset shows the high-magnification FE-SEM image of the tri-layer graphene-laminated micropillar structure. As shown in the figure, the graphene thin film was smoothly laminated on the micropillar-patterned substrate.

In order to verify whether the graphene transferred onto a pillar pattern had been successfully adsorbed, the analysis of confocal Raman spectroscopy with a spatial resolution of 500 nm was performed at three points (A, B, and C). Figure 2(b) shows the representative Raman spectra (532 nm,

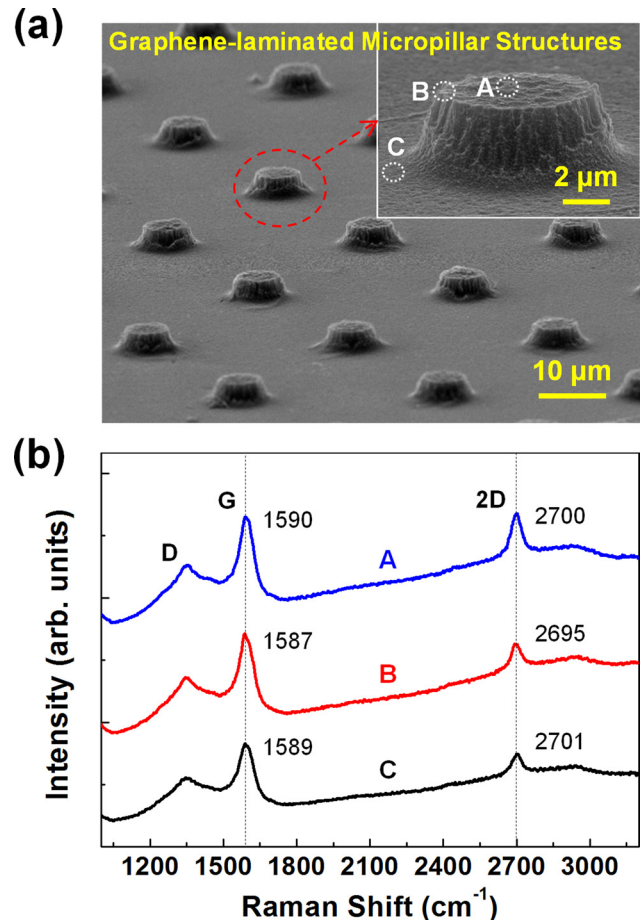


FIG. 2. (a) Low-magnification FE-SEM image of the representative graphene-laminated micropillar array. The inset shows high-magnification FE-SEM images of the representative graphene-laminated micropillar structure, where the dashed circles denote the spatial resolution of the Raman spectra. (b) Raman spectra measured at the positions (A, B, and C) marked in (a).

CRM200, Witec) of the graphene on a micropillar structure. Raman spectroscopy, which is widely used to analyze doping, defect, disorder, stacking, and strain of graphene, allows the analysis of samples in a rapid and facile manner without contacting and destroying them. The main peaks of graphene were the D peak, G peak, and 2D peak. The D peak is from the TO phonon at the K point in the Brillouin zone (BZ), and is activated by the defects and the disorder of points and edges. Meanwhile, the G peak has correlation to the  $E_{2g}$  phonon at the BZ center, and the 2D peak is the second order of the D peak.<sup>25,26</sup> A, B, and C in Figure 2(b), showing points

for the Raman measurement, refer to the center of pillar-shaped upper surface, the side of pillar structure, and the flat surface regions next to the pillar structure, respectively. We observed the spatial variation of the intrinsic structure of the curved graphene-laminated micropillar array, and were able to observe the G and 2D peaks for every measurement point. While G peak and 2D peak were observed at 1590 and 2700  $\text{cm}^{-1}$ , respectively, at point A, G peak, and 2D peak were changed to 1587 and 2695  $\text{cm}^{-1}$  at point B, respectively. G peak and 2D peak at point C were observed at 1589 and 2701  $\text{cm}^{-1}$ , respectively. This result indicates that the adsorption of graphene onto the micropillar pattern was successful. In particular, at point B, the side of a pillar structure, the G peak and 2D peak were red-shifted by 3 and 5  $\text{cm}^{-1}$ , respectively; this is due to the effect of strain produced during the adsorption of graphene onto the micropillar pattern. When graphene is under uniaxial or biaxial strain, the G peak and the 2D peak both exhibit red shifts, while the full width at half maximum of the 2D peak increases.<sup>27,28</sup> On the other hand, at point A, the top of pillar, the strain effect was reduced and the original C state was restored. In other words, with the adsorption of graphene onto micropillar structures, the strain effect was maximized at the side of the structures. Based on the result, the strain was increased 0.23% with the  $-5 \text{ cm}^{-1}$  of 2D peak.

Figure 3(a) shows the schematic illustration of the formation of self-assembled monolayers, HDF-S, onto graphene-laminated micropillar structures. The hydroxyl groups ( $-\text{OH}$ ) of the tri-layer graphene surface formed a strong covalent bond with the surface active group (trichlorosilane- $\text{SiCl}_3$ ) of HDF-S. The self-assembled mono-layers on the graphene were characterized by using ATR-FTIR. As shown in Figure 3(b), compared to the spectrum of pristine graphene, after the deposition of HDF-S, additional peaks at 1147, 1203, and 1235  $\text{cm}^{-1}$  were observed; these peaks were not present in the spectrum of pristine graphene. The abovementioned peak at 1147  $\text{cm}^{-1}$  corresponds to the  $\text{CF}_2$  symmetric, while the 1203 and 1235  $\text{cm}^{-1}$  peaks correspond to asymmetric stretching vibrations.<sup>29-31</sup> This result indicates that the self-assembly of HDF-S on a graphene thin film results in the formation of a CF combination.

Figure 4(a) shows the wetting properties for four different surface conditions: (i) pristine graphene on a flat surface, (ii) pristine graphene on a micropillar array (height of  $\sim 5.1 \mu\text{m}$ ), (iii) HDF-S self-assembled graphene on a flat surface, and (iv) HDF-S self-assembled graphene on a micropillar array (height of  $\sim 5.1 \mu\text{m}$ ). The contact angle was measured at five different points in each sample, and the average and standard deviation were calculated. The columns and error bars represent the average and standard deviation of the measured contact angles. As shown in the figure, the contact angle of the pristine graphene on a flat surface was  $78.8^\circ \pm 0.3^\circ$ , whereas that of the pristine graphene on a micropillar array was  $97.5^\circ \pm 3.7^\circ$ , thus proving that the latter exhibited greater hydrophobicity. The surface roughness of the micropillar structure was higher than that of a flat thin film, resulting in more hydrophobic characteristics. According to the Wenzel model, contact angle is affected by surface roughness as follows:<sup>32</sup>

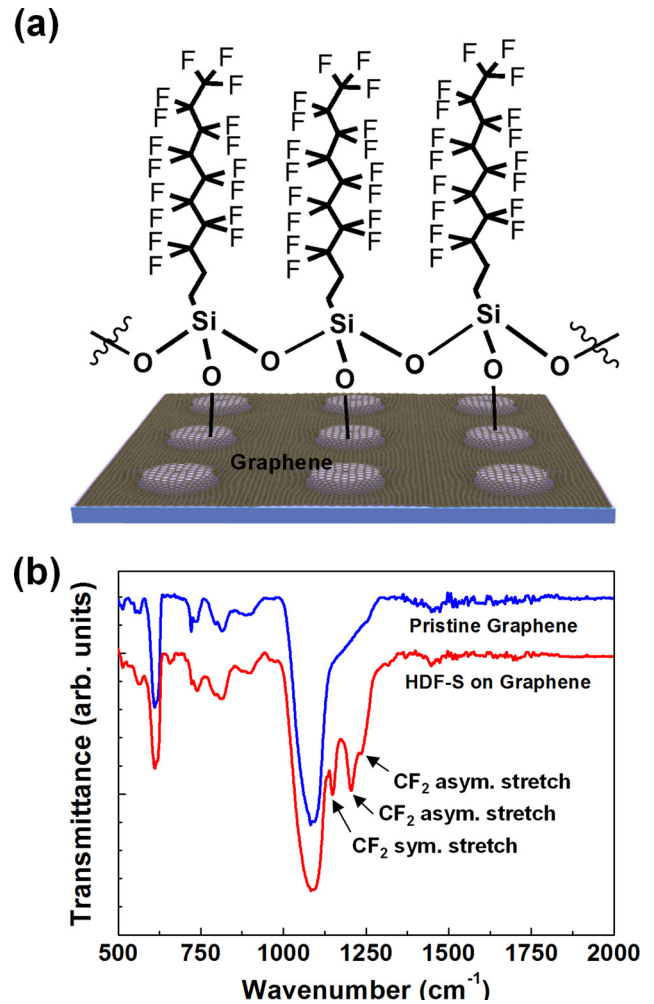


FIG. 3. (a) Schematic illustrating the formation of self-assembled monolayers, HDF-S, onto graphene micropillar structures. (b) ATR-FTIR spectra of graphene surfaces before and after self-assembled monolayers of HDF-S.

$$\cos \theta' = \gamma \cos \theta, \quad (1)$$

where  $\theta$  is the contact angle on a flat surface,  $\theta'$  is the contact angle on a rough surface, and  $\gamma$  is the roughness factor defined as the ratio of the actual area of a rough surface to its geometric projected area. As  $\gamma$  is always greater than 1, hydrophobic characteristics become more pronounced on a rough surface than on a flat surface, and an increase in roughness leads to enhanced hydrophobicity.

After the self-assembly of HDF-S, the contact angles of the HDF-S self-assembled graphene on a flat surface and HDF-S self-assembled graphene on a micropillar array increased to  $98.5^\circ \pm 1.2^\circ$  and  $129.5^\circ \pm 0.7^\circ$ , respectively. The self-assembly of HDF-S results in better contact angle characteristics due to superior hydrophobic characteristics with the hexagonal packing of the functional group  $-\text{CF}_3$  on the top surface. Moreover, contact angle characteristics improved further as the surface topology, micropillar structure, becomes rougher. Contact angles varying with the height of the graphene micropillar structures were observed after HDF-S deposition. As shown in Figure 4(b), the contact angles of graphene-laminated micropillar structures with HDF-S were  $98.5^\circ \pm 1.2^\circ$ ,  $110.5^\circ \pm 3.8^\circ$ ,  $115.5^\circ \pm 3.0^\circ$ ,  $123.4^\circ \pm 1.6^\circ$ , and  $129.5^\circ \pm 0.7^\circ$  (red squares) with heights of 0.0 (flat), 1.7, 2.9,

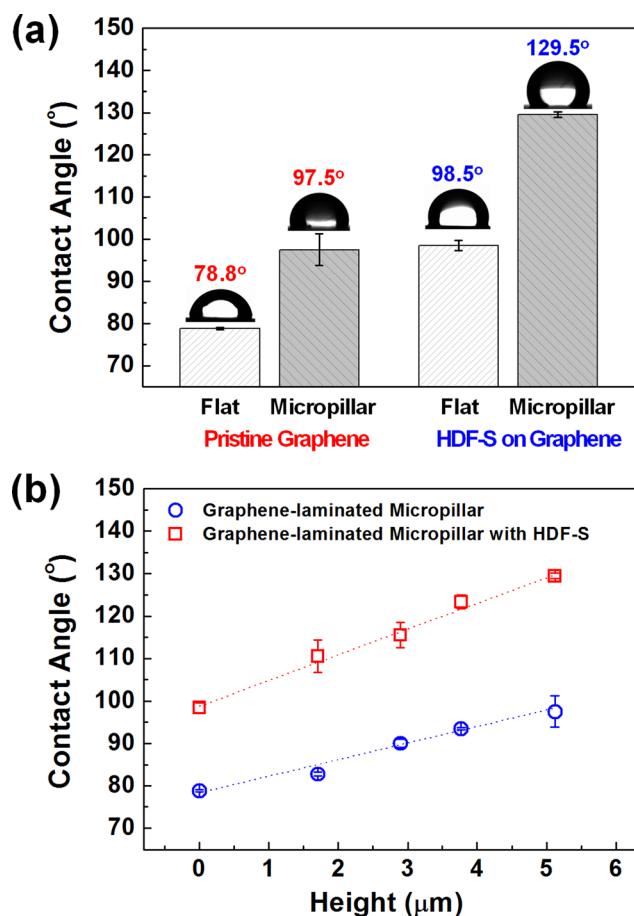


FIG. 4. (a) Wetting properties of (i) pristine graphene on a flat surface, (ii) pristine graphene on a micropillar array, (iii) HDF-S self-assembled graphene on a flat surface, and (iv) HDF-S self-assembled graphene on a micropillar array. (b) Contact angles of HDF-S self-assembled graphene-laminated micropillar structures before and after HDF-S with 5 different heights (0.0 (flat), 1.7, 2.9, 3.8, and 5.1  $\mu\text{m}$ ). The columns and error bars represent the average and standard deviation of the measured contact angles.

3.8, and 5.1  $\mu\text{m}$ , respectively. On the other hand, the contact angles of graphene-laminated micropillar structures without HDF-S were  $78.8^{\circ} \pm 0.3^{\circ}$ ,  $82.8^{\circ} \pm 0.5^{\circ}$ ,  $90.0^{\circ} \pm 0.9^{\circ}$ ,  $93.5^{\circ} \pm 0.3^{\circ}$ , and  $97.5^{\circ} \pm 3.7^{\circ}$  (blue circles) with heights of 0.0 (flat), 1.7, 2.9, 3.8, and 5.1  $\mu\text{m}$ , respectively. Contact angles were enhanced with increasing height of the graphene-laminated micropillar structures.

To prove the outstanding applicability, the slippery property of graphene-laminated micropillar structures with HDF-S was observed by using urea solution. Figure 5(a) shows the time progression of the urea solution sliding down a substrate with HDF-S self-assembled graphene-laminated micropillar arrays (5.1  $\mu\text{m}$ ). Urea solution (1.07 cst at 20  $^{\circ}\text{C}$ , similar level of viscosity as water) used in the experiment was prepared by adding 9.3 g of urea (Sigma-Aldrich), 1.87 g of sodium chloride (Sigma-Aldrich), 1.17 g of sodium (Sigma-Aldrich), and 0.750 g of potassium (Sigma-Aldrich) to 11 of DI water and stirring for 6 h. The urea droplets slid completely without leaving any traces on the HDF-S self-assembled graphene-laminated micropillar structures. Figure 5(b) shows Raman spectroscopy of pristine graphene and HDF-S self-assembled graphene on a micropillar array before and after dropping the urea droplets. After dropping

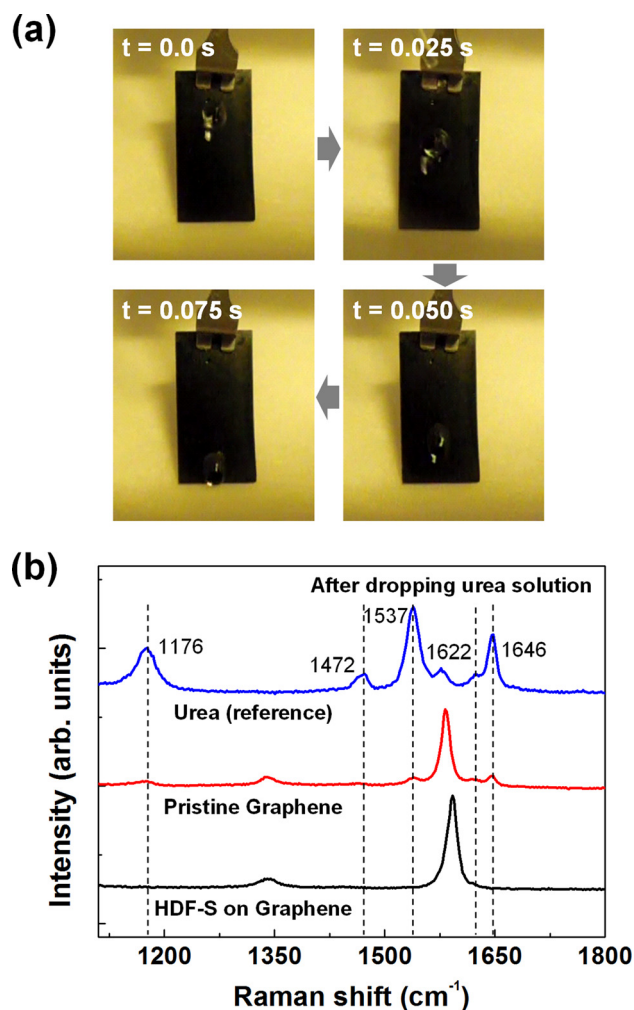


FIG. 5. (a) Time sequence images showing the slippery properties of the HDF-S self-assembled graphene-laminated micropillar structure (height of 5.1  $\mu\text{m}$ ) using urea solution. (b) Raman spectroscopy of pristine graphene and HDF-S self-assembled graphene on a micropillar array before and after dropping the urea droplets.

urea solution droplets 50 times on pristine graphene-based and HDF-S self-assembled graphene-based micropillar structures, the residue of urea was observed only on pristine graphene-based micropillar structures, but not on HDF-S self-assembled graphene-based micropillar structures. The observed five main peaks, 1176, 1472, 1537, 1622, and 1646  $\text{cm}^{-1}$ , on pristine graphene-based micropillar structures after dropping urea solution are  $\text{NH}_2$  rocking vibration, CO stretching vibration, CN asymmetric stretching vibration,  $\text{NH}_2$  asymmetric in plane bending vibration, and  $\text{NH}_2$  deformation vibration, respectively.<sup>33,34</sup> The result supports that the residue of urea was not remained on the surface of HDF-S self-assembled graphene-based micropillar array. This result indicates that the hydrophobic graphene-laminated micropillar structure developed in this study could have significant potential applications for bionic devices.

## CONCLUSIONS

In summary, graphene-laminated micropillar structures were fabricated and their wetting properties were improved by increasing the height of the structure and employing the

HDF-S based SAMs. The graphene can be stretched and fully laminated on the micropillar array. The graphene-laminated micropillar structures with HDF-S show hydrophobic properties (contact angle of  $129.5^\circ$ ) compared to pristine graphene ( $78.8^\circ$ ) on a flat surface, pristine graphene on micropillar structures ( $97.5^\circ$ ), and HDF-S coated graphene ( $98.5^\circ$ ) on a flat surface. This result can be explained by a synergistic effect of an increased surface roughness in the graphene-laminated structure and a created fluorocarbon SAM, which could reduce the surface energy on the graphene surface. Graphene laminates and HDF-S self-assembly techniques could be well-suited to increase hydrophobicity and slipperiness on bionics, satellite antennas, building windows, solar collector panels, ship exteriors, and the interior of pipes.

## ACKNOWLEDGMENTS

This research was supported by the Basic Science Research Program (2012R1A2A2A01013734) and the Public Welfare and Safety Research Program (2013M3A2A1067519) through the National Research Foundation of Korea (NRF) funded by the Ministry of Science, ICT and Future Planning.

- <sup>1</sup>Y.-M. Lin, C. Dimitrakopoulos, K. A. Jenkins, D. B. Farmer, H.-Y. Chiu, A. Grill, and Ph. Avouris, *Science* **327**, 662 (2010).
- <sup>2</sup>L. Liao, Y.-C. Lin, M. Bao, R. Cheng, J. Bai, Y. Liu, Y. Qu, K. L. Wang, Y. Huang, and X. Duan, *Nature* **467**, 305 (2010).
- <sup>3</sup>T. Mueller, F. Xia, and P. Avouris, *Nat. Photonics* **4**, 297 (2010).
- <sup>4</sup>G. Konstantatos, M. Badioli, L. Gaudreau, J. Osmond, M. Bernechea, F. P. G. de Arquer, F. Gatti, and F. H. L. Koppens, *Nat. Nanotechnol.* **7**, 363 (2012).
- <sup>5</sup>J. Yan, M.-H. Kim, J. A. Elle, A. B. Sushkov, G. S. Jenkins, H. M. Milchberg, M. S. Fuhrer, and H. D. Drew, *Nat. Nanotechnol.* **7**, 472 (2012).
- <sup>6</sup>K. Krishnamoorthy, M. Veerapandian, L. H. Zhang, K. Yun, and S. J. Kim, *J. Phys. Chem. C* **116**, 17280 (2012).
- <sup>7</sup>Y. Zhang, S. F. Ali, E. Dervishi, Y. Xu, Z. Li, D. Casciano, and A. S. Biris, *ACS Nano* **4**, 3181 (2010).
- <sup>8</sup>K. Y. Yeh, K.-H. Cho, and L.-J. Chen, *Langmuir* **25**, 14187 (2009).
- <sup>9</sup>A. Tuteja, W. Choi, J. M. Mabry, G. H. McKinley, and R. E. Cohen, *Proc. Natl. Acad. Sci. U.S.A.* **105**, 18200 (2008).
- <sup>10</sup>L. Huang, S. P. Lau, H. Y. Yang, E. S. P. Leong, S. F. Yu, and S. Praver, *J. Phys. Chem. B* **109**, 7746 (2005).
- <sup>11</sup>X. Song, J. Zhai, Y. Wang, and L. Jiang, *J. Phys. Chem. B* **109**, 4048 (2005).
- <sup>12</sup>T. Nishino, M. Meguro, K. Nakamae, M. Matsushita, and Y. Ueda, *Langmuir* **15**, 4321 (1999).
- <sup>13</sup>A. Nakajima, K. Hashimoto, and T. Watanabe, *Monatsh. Chem.* **132**, 31 (2001).
- <sup>14</sup>T. N. Van, Y. K. Lee, J. Lee, and J. Y. Park, *Langmuir* **29**, 3054 (2013).
- <sup>15</sup>Y. Park, M. Han, and Y. Ahn, *Bull. Korean Chem. Soc.* **32**, 1091 (2011).
- <sup>16</sup>R. Hensel, R. Helbig, S. Aland, A. Voigt, C. Neinhuis, and C. Werner, *NPG Asia Mater.* **5**, e37 (2013).
- <sup>17</sup>T.-S. Wong, S. H. Kang, S. K. Y. Tang, E. J. Smythe, B. D. Hatton, A. Grinthal, and J. Aizenberg, *Nature* **477**, 443 (2011).
- <sup>18</sup>J. Rafiee, X. Mi, H. Gullapalli, A. V. Thomas, F. Yavari, Y. Shi, P. M. Ajayan, and N. A. Koratkar, *Nat. Mater.* **11**, 217 (2012).
- <sup>19</sup>Z. Li, Y. Wang, A. Kozbial, G. Shenoy, F. Zhou, R. McGinley, P. Ireland, B. Morganstein, A. Kunkel, S. P. Surwade, L. Li, and H. Liu, *Nat. Mater.* **12**, 925 (2013).
- <sup>20</sup>Y. J. Shin, Y. Wang, H. Huang, G. Kalon, A. T. S. Wee, Z. Shen, C. S. Bhatia, and H. Yang, *Langmuir* **26**, 3798 (2010).
- <sup>21</sup>Z. Lin, Y. Liu, and C.-P. Wong, *Langmuir* **26**, 16110 (2010).
- <sup>22</sup>X. Li, Y. Zhu, W. Cai, M. Borysiak, B. Han, D. Chen, R. D. Piner, L. Colombo, and R. S. Ruoff, *Nano Lett.* **9**, 4359 (2009).
- <sup>23</sup>X. Liang, B. A. Sperling, I. Calizo, G. Cheng, C. A. Hacker, Q. Zhang, Y. Obeng, K. Yan, H. Peng, Q. Li, X. Zhu, H. Yuan, A. R. H. Walker, Z. Liu, L. Peng, and C. A. Richter, *ACS Nano* **5**, 9144 (2011).
- <sup>24</sup>J.-H. Park, W. Jung, D. Cho, J.-T. Seo, Y. Moon, S. H. Woo, C. Lee, C.-Y. Park, and J. R. Ahn, *Appl. Phys. Lett.* **103**, 171609 (2013).
- <sup>25</sup>A. C. Ferrari, *Solid State Commun.* **143**, 47 (2007).
- <sup>26</sup>L. M. Malard, M. A. Pimenta, G. Dresselhaus, and M. S. Dresselhaus, *Phys. Rep.* **473**, 51 (2009).
- <sup>27</sup>T. M. G. Mohiuddin, A. Lombardo, R. R. Nair, A. Bonetti, G. Savini, R. Jalil, N. Bonini, D. M. Basko, C. Galiotis, N. Marzari, K. S. Novoselov, A. K. Geim, and A. C. Ferrari, *Phys. Rev. B* **79**, 205433 (2009).
- <sup>28</sup>J. Zabel, R. R. Nair, A. Ott, T. Georgiou, A. K. Geim, K. S. Novoselov, and C. Casiraghi, *Nano Lett.* **12**, 617 (2012).
- <sup>29</sup>K. K. S. Lau, J. A. Caulfield, and K. K. Gleason, *Chem. Mater.* **12**, 3032 (2000).
- <sup>30</sup>M. Inayoshi, M. Hori, T. Goto, M. Hiramatsu, M. Nawata, and S. Hattori, *J. Vac. Sci. Technol., A* **14**, 1981 (1996).
- <sup>31</sup>C. I. Butoi, N. M. Mackie, L. J. Gamble, D. G. Castner, J. Barnd, A. M. Miller, and E. R. Fisher, *Chem. Mater.* **12**, 2014 (2000).
- <sup>32</sup>R. N. Wenzel, *J. Phys. Chem.* **53**, 1466 (1949).
- <sup>33</sup>R. Keuleers, B. Rousseau, C. Van Alsenoy, and H. O. Desseyn, *J. Phys. Chem. A* **103**, 4621 (1999).
- <sup>34</sup>R. L. Frost, J. Kristof, L. Rintoul, and J. T. Klopogge, *Spectrochim. Acta Part A* **56**, 1681 (2000).